Three-Dimensional Inviscid Flow in Mixers, Part I: Mixer Analysis Using a Cartesian Grid

T. J. Barber*
United Technologies Research Center, East Hartford, Connecticut
G. L. Muller† and S. M. Ramsay‡
Pratt & Whitney Aircraft Group, East Hartford, Connecticut
and
E. M. Murman¶
Massachusetts Institute of Technology, Cambridge, Massachusetts

A three-dimensional potential flow analysis has been formulated and applied to the inviscid flow over a turbofan forced mixer. In Part I, a method using a novel small disturbance formulation is presented which analytically uncouples the circumferential flow from the radial and axial flow problem, thereby reducing the analysis to the solution of a series of axisymmetric problems. These equations are discretized using a flux volume formulation along a Cartesian grid. The method extends earlier applications of the Cartesian method to complex cambered multicomponent geometries. Calculations are presented for a symmetric mixer in a planar duct. Good agreement is obtained with a small disturbance singularity superposition analysis. In Part II, the method is extended to treat flows with different energy levels and applied to experimentally tested turbofan forced mixer geometries.

Nomenclature

A = area of elemental face
C_p = pressure coefficient
g_k = kth component of axisymmetric perturbation potential
h_k = kth component of angular portion of perturbation potential
i_x, i_r, i_θ = unit vectors in cylindrical coordinates
K = separation of variables parameter
L = axial length of mixer lobe
M = Mach number
n = normal component
NH = number of flux equations solved
p = static pressure
R_m = mean radius
x, r, θ = cylindrical coordinates
u, v, w = velocity components
β = compressibility factor
Γ = circulation at lobe trailing edge
ϵ = geometry scaling parameter
λ_k = kth Fourier component of lobe surface
ψ = perturbation velocity potential

Subscripts

$E, W,$ = property in x direction
i, j = (x,r) difference indices
k = Fourier harmonic component
S, N = property in r direction
U, L = upper and lower component of flux element
o = stagnation property
x, r, θ = partial derivatives in (x,r,θ) coordinate
∞ = inlet property

Received Aug. 5, 1985; revision received Jan. 22, 1986.

*Senior Research Engineer. Member AIAA.
†Senior Analytical Engineer. Member AIAA.
§Analyst.
¶Professor of Aeronautics and Astronautics. Member AIAA.

Introduction

THE numerical treatment of internal flow problems has reached a level of maturity such that two- and three-dimensional solutions of cascade and duct/gas path problems can be considered sufficiently realistic and reliable to be utilized in a preliminary design system. In these situations, physical and geometrical simplifications have been introduced to make the problem more tractable, while still retaining the essential features of the problem. Extension of these techniques to more complicated phenomenological and geometrical problems represents the current thrust of many gas turbine related research efforts. The analysis of the turbofan forced mixer flowfield represents one such problem.

A forced mixer is a device used in gas turbine engines to internally mix the hot core or primary gas stream with the cold fan bypass or secondary stream upstream of the nozzle exit plane. Conventional or commercial forced mixer configurations consists of a periodic lobe structure that can be described in terms of a number of geometric features. Figure 1 illustrates two cross-sectional views of a typical forced mixer configuration. For many years, mixer configurations were designed using a trial and error experimental approach in which limited traverse and performance data were used to refine design concepts.[1-3] More recently, "benchmark" experiments[4,5] have utilized high response and LDV instrumentation to probe the mixing chamber in an attempt to explain the driving mechanisms of the mixing process. These experiments indicate that the mixing process is principally inviscid, and the primary mixing mechanism is the secondary flow generated in the lobed region of the flow. The analysis shown in this paper presents a technique applicable to the solution of this geometrically complex flow problem and demonstrates its utility by analyzing the flow over a forced mixer.

Analytical Approach

Overview

The forced mixer consists of a convoluted lobe section and a mixing chamber. Observations have proven that the lobe region is responsible for the secondary flow generation which

drives the mixing process in the downstream duct region to the nozzle exit plane. The convoluted lobes can be viewed as a ring wing with a periodic "spanwise" loading distribution $\Gamma(\theta)$, as is shown in Fig. 2. The periodic lobe cambering produces a nonuniform loading distribution and a corresponding shed vorticity field whose strength varies periodically in θ. The shed vortex is associated with a cross-flow velocity field (secondary flow) that "mixes" the flow as it is convected downstream. The vorticity is then stretched and eventually dissipated in the mixing chamber through the action of viscosity.

A complete inviscid treatment of the three-dimensional lobe region is still a difficult problem due to geometric complexity, multiple energy streams, and compressibility. It is reasonable, therefore, to propose a zonal analytical approach, wherein regions are treated using techniques which are applicable in each zone. In such an approach it is possible to consider the lobe problem using a simpler inviscid potential analysis. Although power addition must be considered in the engine environment, the flow can still be considered as two separate *irrotational* regions separated by a vortex sheet. In order to retain a potential formulation, the wake/vortex sheet must be dynamically tracked. Any use of a body conforming grid however would require the solution algorithm to also dynamically update the conforming grid. The algorithm described below proposes an alternate approach to this problem.

As shown in Fig. 2, the mixer lobe is characterized by two length scale ratios, which provide relative measures for the lobe height, axial and azimuthal variations

$$\epsilon_1 = (\Delta R/L), \qquad \epsilon_2 = (N\Delta R/2\pi R)$$

where N is the number of lobes, L the axial length, and ΔR the lobe height above a mean reference radius. For many current designs, mixer lobes are axially slender ($\epsilon_1 \ll 1$), and local Mach numbers are low enough that a small disturbance model can be introduced as a means for treating the salient features of the lobe mixer problem. In the next section a small disturbance formulation is developed that analytically uncouples the θ variation and reduces the problem to the solution of a sequence of axisymmetric problems. These axisymmetric problems can be solved by taking advantage of previous experience[6] in which the effects of power addition and "exact" surface boundary conditions were modeled. In contrast to this earlier work, a finite volume cylindrical grid formulation similar to that of Wedan and South[7] is used. This approach yields a straightforward treatment of the mixer problem which contains a number of geometric and flow features that are more complex than the symmetric geometries analyzed in Ref. 7.

The power contribution and lobe loading result in a potential jump $[\varphi]$ across the wake shed from the lobe trailing edge. The corresponding induced secondary flow has a net circulation Γ. By an appropriate choice of the closed path of integration over half a lobe, shown in Fig. 3, the circulation integral reduces to

$$\Gamma = [\varphi]_{\theta=0} - [\varphi]_{\theta=\theta_0} \tag{1}$$

In the following sections, a potential flow analysis for the forced mixer is developed. The complex three-dimensional problem previously described is linearized permitting an uncoupling of its θ dependence in the governing equations. Special treatment of surface and Kutta conditions however is needed to insure compatibility with the governing equations and the physics of the problem, while also uncoupling their θ dependence. The extension of this potential flow analysis to include power effects is treated in Part II.

Potential Flow Analysis

The inviscid flow analysis will be applied to the flow domain between the fan and core flow discharge plane and a downstream plane in the mixing chamber, schematically shown in Fig. 4. In the present work, this plane has been chosen upstream from the nozzle exit plane to avoid both nonlinear compressibility and viscous mixing effects. The governing equation of mass conservation, applied to an arbitrary control volume in space, yields

$$\int \rho \vec{v} \cdot \vec{n} \, dA = 0 \tag{2}$$

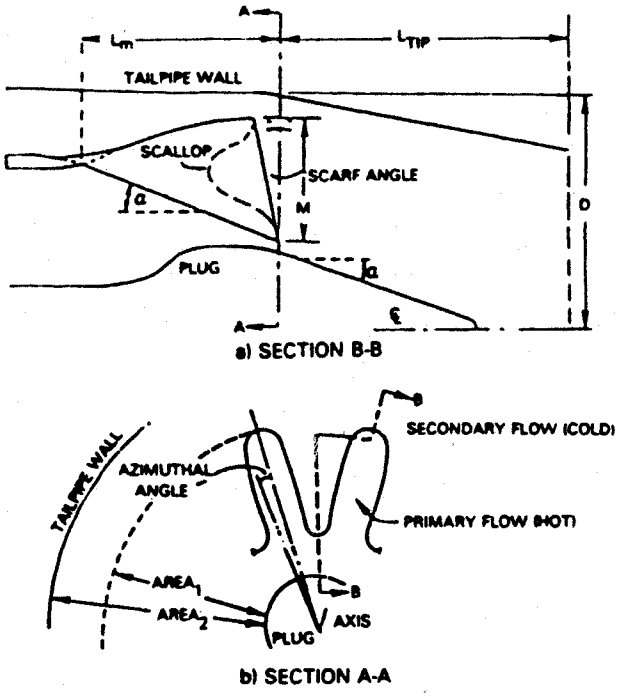

Fig. 1 Mixer wake geometry definition.

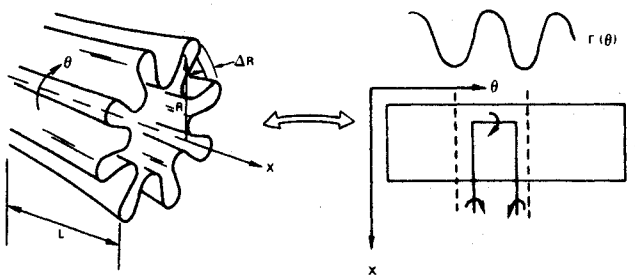

Fig. 2 Ring wing analog of forced mixer.

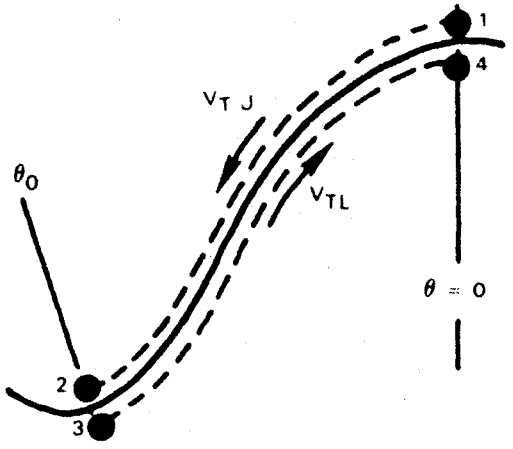

Fig. 3 Schematic of lobe trailing edge integration path.

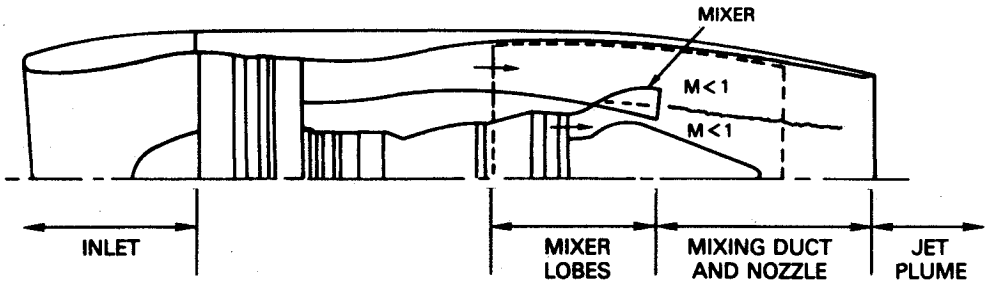

Fig. 4 Mixed flow nacelle analysis domain.

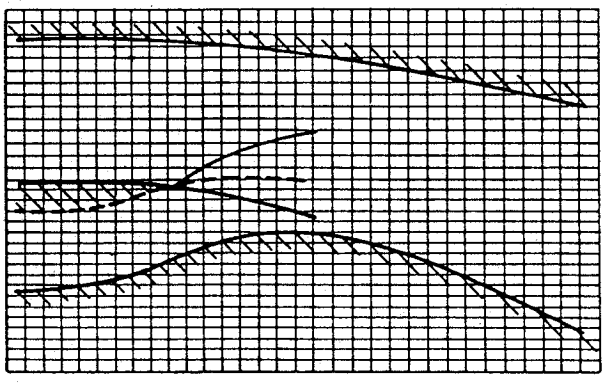

Fig. 5 Angular slice of cylindrical grid intersecting duct walls.

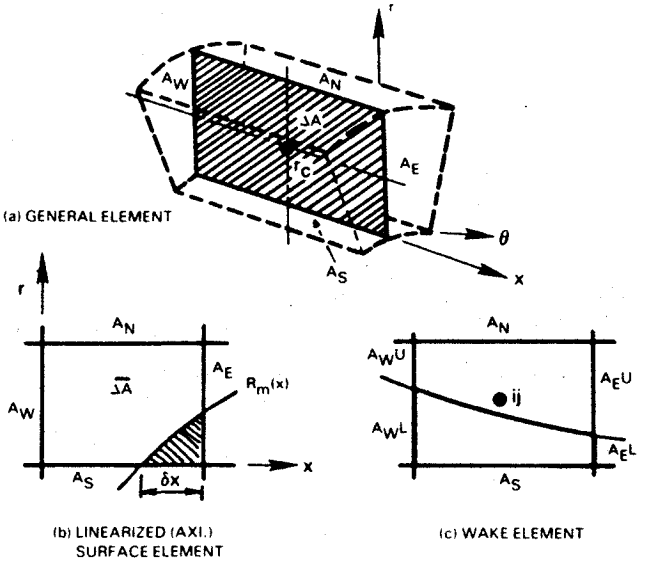

Fig. 6 Cartesian flux volume element description.

The nondimensional mass flux is defined in terms of a perturbed flow from an upstream subsonic x-"aligned" flow as follows:

$$\rho\vec{v} = (1+\beta^2\varphi_x)\vec{i}_x + \varphi_r\vec{i}_r + (1/r)\varphi_\theta\vec{i}_\theta \tag{3}$$

where $\beta^2 = 1-M_\infty^2$ and φ is the perturbation velocity potential. The β^2 term reflects an approximation treatment of compressibility effects in the problem. Only the linear or first order terms have been retained in Eq. (3). The expansion is made assuming that all surfaces have slender shapes in the streamwise direction ($\epsilon_1 \ll 1$).

Appropriate surface boundary conditions can be derived from a flow tangency condition given by

$$\vec{v}\cdot\nabla F = 0 \tag{4}$$

where the velocity vector $\vec{v}$ is given in terms of a velocity potential, and F is a general surface described in terms of the r,θ,x cylindrical coordinate system

$$F(r,x,\theta) = r - f(x,\theta) = 0 \tag{5}$$

If a perturbation velocity potential is assumed, then the corresponding perturbation velocity components can be considered small relative to the upstream flow. The mixer lobe surface [Eq. (5)] is also assumed to be perturbed about some mean surface $R_m(x)$ midway between the lobe crest and trough; therefore, the flow tangency condition can be approximated by

$$\varphi_r = f_x + (f_\theta/R_m^2)\varphi_\theta \tag{6}$$

The perturbation or small disturbance approximation is equivalent to limiting surface slopes to order ϵ_1. This linearization of the boundary condition is needed to render the overall problem separable, as will be shown in the next section. At first glance, it appears that the last term in Eq. (6) is of order ϵ_1^2; however, no such perturbation restriction has been imposed in the azimuthal direction. The terms f_x and f_θ are known functions which describe the lobe geometry.

Problem closure is obtained by imposing a quasi one-dimensional analysis for definition of the inlet flux and a Kutta condition at the lobe trailing edge to uniquely set the net circulation.

Separation of Variables and Cartesian Grid Approach

In order to simplify the analysis, a cylindrical coordinate system orientation is used to evaluate the flux integral in Eq. (2). By evaluating the flux integrals on a Cartesian grid, the numerical algorithm developed herein will be applicable to a broad class of two- and three-dimensional problems that do not lend themselves to more conventional body wrapped grids. In such an approach, one can substitute the complexity of boundary/mesh intersections for the complexity of multielement body mesh generation. An angular cut for a typical internal mixer flow application of this grid is shown on Fig. 5. For the particular application presented in this paper, the mixer lobe geometry is assumed, for simplicity, to have a trailing edge aligned with the mesh.

The mixer lobe can be considered a general three-dimensional lobed surface perturbed about some mean surface. It is possible to avoid analyzing the full three-dimensional problem by recognizing that the flow is a periodic function of the number of lobes. Solutions to the linear governing Eq. (2) can be separated, i.e.,

$$\psi(x,r,\theta) = g(x,r)\ h(\theta) \tag{7}$$

It will subsequently be shown that the nonlinear aspects of the surface definition and the surface boundary condition are also separable. Separating out the θ dependence will reduce the analysis to a series of axisymmetric problems on a Cartesian grid.

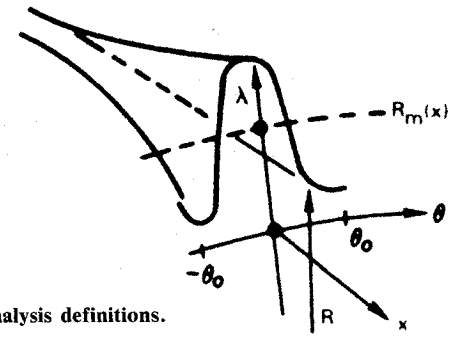

Fig. 7 Moment analysis definitions.

Flux Volume Formulation

Combining Eqs. (2-4), the governing flux balance equation terms can be approximately separated into terms that are either a function of (r,x) or of θ alone,

$$\frac{{}_{E\text{-}W}\int \beta^2 g_x r\,dr + {}_{N\text{-}S}\int r g_r\,dx}{{}_{\Delta A}\int g(dr\,dx/r)} = \frac{-h_\theta}{\int h\,d\theta} = K^2 \tag{8}$$

where K is the separation constant and the *E-W*, *N-S*, and ΔA integrals are the appropriate flux balance integrals on an elemental volume evaluated in the (x,r) plane shown in Fig. 6. The θ dependence of Eq. (8) can be recast to identify the periodic nature of the separated variable. The solution for $h(\theta)$ includes linear combinations of trigonometric functions, where appropriate application of the symmetry boundary condition at the lobe crest simplifies this to

$$h_k = B_k \cos[(k\pi\theta/\theta_0)], \qquad k=0,1,2,\ldots NH \tag{9}$$

where $K = k\theta/\theta_0$, θ_0 is the half angle of the lobe (crest to trough), NH the number of harmonics used in the Fourier series, and B_k a sequence of unknown coefficients still to be determined. The $k=0$ solution corresponds to the axisymmetric solution limit. Since the separation constant can take on multiple values, the potential assumes a more general form

$$\psi = \sum_k g_k h_k$$

The axisymmetric dependence of Eq. (8) can be evaluated for an arbitrary point in the flowfield on integrals aligned to the cylindrical mesh (Fig. 6a) to produce

$$\int_{E\text{-}W} \beta^2 g_{x_k} r\,dr + \int_{N\text{-}S} g_{r_k} r\,dx - K^2 \int\int_{\Delta A} \frac{1}{r} g_k\,dr\,dx = 0 \tag{10}$$

The last integral is a source term integrated over the enclosed area $(dr\,dx)$. Evaluating the flux balance Eq. (10) on an arbitrary flow element yields

$$-(\beta^2 g_{x_k})_W A_w + (\beta^2 g_{x_k})_E A_E + (g_{r_k})_N A_N - (g_{r_k})_S A_S - g_k(K^2 \Delta A/r_c) = 0$$
$$k=0,1,2,\ldots NH \tag{11}$$

where the r term has been approximated by its value at the center of each flux cell. Equation (11) is a discrete approximation whose subscripts refer to the respective faces of the elemental volume shown on Fig. 6a. Central differencing of the flux terms and collecting the contributions at each node results in a tridiagonal equation system in terms of $g_{i,j,k}$, where i refers to an index along the x axis and j an index along the r axis.

$$A_j g_{i,j-1,k} + B_j g_{i,j,k} + C_j g_{i,j+1,k} = W_{j,k}$$
$$k=0,1,2,\ldots NH \tag{12}$$

Closure of the problem formulation requires application of boundary conditions on the boundaries of the domain of integration. Referring to the computational outline in Fig. 5, the flow tangency condition will be imposed on all solid surfaces. The upstream flows normally are defined in terms of the engine discharge conditions, but flow continuity (Kutta condition) at the lobe trailing edge necessitates an alternate approach to avoid overspecifying the inlet conditions. These boundary conditions will be explained in the following sections.

Surface Boundary Condition

In a flux formulation, the surface boundary condition is implemented as a zero flux condition on all solid surfaces. The flux balance for an element intersecting the three-dimensional lobe surface is not separable along the general lobe surface. In order to render the problem separable, the boundary conditions are also linearized as previously shown for a general element, and the θ dependence is removed resulting in a modified boundary condition with a sourcelike term applied on a mean axisymmetric surface, $R_m(x)$. The surface intersecting computational flux volume element is shown in Fig. 6b. The flux balance on such an element must be modified by an additional source term representing the "surface" flux $(\bar{g}_r)$ in the r direction,

$$\int_{E\text{-}W} \beta^2 g_{x_k} r\,dr + \int_{N\text{-}S} g_{r_k} r\,dx - \int_{RM} \bar{g}_{r_k} r\,dk - K^2 \int_{\Delta\bar{A}} g_k(dr\,dx/r) = 0$$
$$k=0,1,2\ldots NH \tag{13}$$

The areas in the integrals describe only the external portion of the cell on the side and azimuthal $(\Delta\bar{A})$ faces.

By applying the mean radius approximation to the surface contour, one can also express the lobe surface in terms of separable variables, i.e.,

$$f(x,\theta) = R_m(x) + \sum_{k=1}^{NH} \lambda_k(x) h_k(\theta) = \sum_{k=0}^{NH} \lambda_k(x) h_k(\theta) \tag{14}$$

where $\lambda_o(x)$ is the axisymmetric modal shape and may be used as a mean radius. A Fourier moment analysis couples the θ dependence of the contour with radial variation dependent variables. The unknown coefficients λ_k are determined by using the angular definition shown on Fig. 7.

$$\lambda_k(x) = \frac{1}{\theta_o}\int_{-\theta_o}^{\theta_o} f(x,\theta)\cos\left(\frac{k\pi\theta}{\theta_o}\right) d\theta$$

Substitution of the modal description of the geometry given in Eq. (14) into the surface boundary condition and taking advantage again of the orthogonality of alternate Fourier modes for the g_k's on the boundary, reduces the surface boundary condition to a flux along a mean surface which is given by

$$\bar{g}_{r_k}(x,R_m) = \lambda_k'(x) + \frac{1}{2R_m^2}\sum_j \sum_n \lambda_n(x) g_j(x,R_m)\cdot[\delta_{k,n-j} - \delta_{k,n-j}]$$
$$k=0,1,2,\ldots NH \tag{15}$$

where δ_{ij} is the Kronecker delta function. The first term on the right side is the primary contribution to the effective sur-

face flux to a given mode. The second term represents a coupling of the different modal solutions due to the product $f_\theta \psi_\theta$ in Eq. (13). If parameter ϵ_2 is small, this term is absent. Observe that Eq. (15) is a mixed type boundary condition, therefore, the solution algorithm cannot explicitly determine the $g_k(r,x)$'s from the given boundary conditions. This problem of coupled modal equations is alleviated by lagging the alternate modes in the iterative solution that will be discussed shortly.

The modal solutions for the functions $g_k(x,r)$ can be discretized along the cylindrical mesh to yield

$$-\beta^2 g_{x_{k_W}} A_w + \beta^2 g_{x_{k_E}} A_E + g_{r_{k_N}} A_N - g_{r_{k_S}} A_S - \bar{g}_{r_k} \bar{R}_m \delta_x - \frac{K^2}{R_m} g_k \overline{\Delta A} = 0$$

$$k = 0,1,2,\ldots NH. \tag{16}$$

where A denotes the exterior portions of the areas of the intersected cells and $\overline{\Delta A}$ the exterior area of its azimuthal face as shown in Fig. 6b. Equation (16) is a direct analog to the general flux balance in Eq. (8), with the surface effect modifying the effective element face over (ΔA) and a flux term representing the effect of the surface on the Cartesian cell balance. In general, a surface element includes a region of flow and a region interior to the body. Along the mean surface however, an element includes a core flow and fan flow region. Correct flux balancing in each region is expedited by tracking the potentials of each flow separately across the surface.

The discretization of the boundary Eqs. (15) and (16) is complicated by the mixed mode term in the "surface" flux. In order to solve the equations numerically, the coupled term is included as a known function in the flux balance. This term therefore is grouped in the right side of the tridiagonal equation (9) and lagged in the iterative solver, i.e.,

$$W'_{j,k} = W_{j,k} + \bar{R}_m \delta x \left[\lambda'_k + (G_2 / 2R_m^2) \right] \tag{17a}$$

$$B'_j = B_j + (\bar{R}_m \delta x G_1 / 2R_m^2) \tag{17b}$$

where G_1 and G_2 are the coefficients from Eq. (15) of the kth mode and the mixed modes (minus the kth term), respectively.

Solution Algorithm

The governing equations and boundary conditions reduce the analysis problem to a system of linear algebraic equations in terms of the $g_k(x,r)$'s and correspondingly the velocity potential. These equations are solved iteratively using a successive line over-relaxation procedure (SLOR). To optimize the calculations, a grid halving algorithm is utilized. In such an algorithm, the previous coarse grid solution is interpolated onto the next or finer grid as its initial guess. The solution convergence on each grid is monitored by tracking either the residual, defined as the normalized error in the mass conservation equation at the nth iterate, or the jump in potential at the splitter trailing edge. Typically the residual is a monotonically decreasing function and is reduced about two orders of magnitude on each grid. Finally, the results are displayed in terms of the pressure coefficient defined for each stream relative to its own upstream dynamic head.

Flow Boundary Conditions

Flow closure boundary conditions for the governing equations are set by specifying the net flow rate at the nozzle exit plane, while a Kutta condition at the lobe trailing edge defines the relative flow split between the streams above and below the mixer. Assuming the flow at the inlet and exit planes can be modeled by a quasi-one-dimensional flow, a unique flow split is determined from a simple Newton iteration scheme. This directly determines g_x for each stream at the downstream plane of the computational domain. The details of the method are given more completely in Part II.

The inviscid interaction of the flow streams downstream of the lobe surface is controlled by vortex sheet whose initial strength is set by a Kutta condition at the trailing edge. This vortex sheet is convected from the lobe trailing edge as a constant jump in potential and will follow the trailing edge streamline. The two streams interact through the local potential jump that is determined from the basic consistency conditions across a contact discontinuity, i.e., static pressure match on the wake or vortex sheet S_w and streamline slope continuity

$$\vec{v} \cdot \vec{n} = 0 \text{ on } S_W^+, S_W^-$$

Basic linear theory assumes the wake lies along a constant radius surface from the trailing edge, and consistent with the surface boundary condition formulation, the streamline slope condition is relaxed by assuming that the wake can be modeled by a mean constant radius surface or an axisymmetric surface that varies with axial position. Flow is permitted to cross through the constant radius. Consider the mass flux balance on an element that includes an arbitrarily oriented mean wake streamline (Fig. 6c). Application of the flux balance (16) to the upper and lower portions of the (ij) wake elements results in equations that assume that a mass flux can exist across the given wake contour. Adding the conservation components will produce an equation for the ijth element where the flux contributions across the wake [g_r] identically cancel each other out. If the potentials corresponding to the flux balances taken on the two sides of the wake are defined in terms of a mean potential and a potential jump (g_k) as follows

$$\bar{g}_{i,j,k} = \tfrac{1}{2} (g^U_{i,j,k} + g^L_{i,j,k}) \tag{18a}$$

$$[g_k]_{ij} = (g^U_{i,j,k} - g^L_{i,j,k}) \tag{18b}$$

then the flux balance for a wake element becomes

$$A^L_j \bar{g}_{i,j-1,k} + (B^U_j + B^L_j) \bar{g}_{i,j,k} + C^U_j \bar{g}_{i,j,k} = W^U_{jk} + W^L_{jk} - [g_k]_{ij} (B^U_j - B^L_j) \tag{19a}$$

This equation corresponds to one row in the general

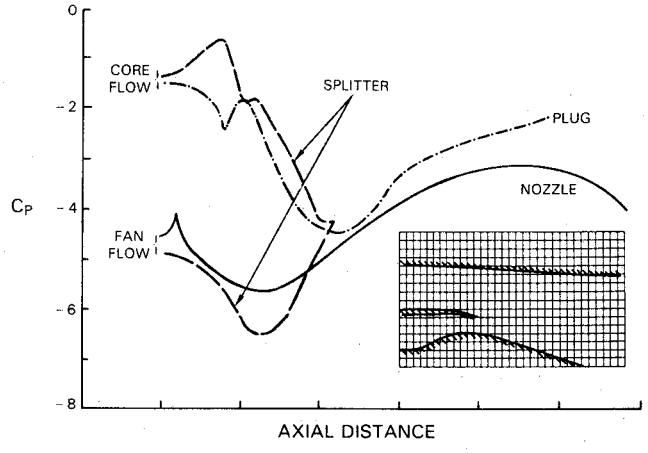

Fig. 8 Surface static pressure coefficient distribution over an unpowered axisymmetric configuration.

This equation corresponds to one row in the general $(JM \times JM)$ tridiagonal matrix for the ith line,

$$\begin{vmatrix} \cdots & \cdots & \cdots & & & \\ A_{j-1} & B_{j-1} & C_{j-1} & & & \\ A_j^L & (B_j^L + B_j^U) & C_j^U & & & \\ & & & & & \\ A_{j+1} & B_{j+1} & C_{j+1} & & & \\ & & & & & \\ \cdots & \cdots & \cdots & & & \end{vmatrix} \tag{19b}$$

$$\begin{vmatrix} A_{j-2} & B_{j-2} & C_{j-2} & & & \\ & A_{j-1} & B_{j-1} & C_{j-1} & & \\ & & A_j^L & B_j^L & 0 & C_j^U \\ & & & 0 & B_j^U & \\ & & & & A_{j+1} & B_{j+1} & C_{j+1} \end{vmatrix} \tag{19c}$$

The two new (jth) equations are similar to the individual wake element flux balances with the added proviso that the alternate off-diagonal term are zero. This is equivalent to assuming that the wake is a solid boundary since all solid boundary surfaces contribute zero flux to the net balance. Under such a format, the program can automatically treat these constructed equations in the algorithm and the wake equation is arrived at by contracting or adding the appropriate equations. It is important to note this dual potential technique isolates the upper and lower flows by an effective solid surface. This method, therefore, also resolves the flux cell problem arising when slender surfaces (relative to the computational mesh spacing) pass through the middle of a cell and produce flow domains in that cell.

The matrix solution for the ith axial row requires an algorithm for defining the $[g_k]$. The potential jump is obtained by applying the constraints of static pressure

$$p^U = p^L \tag{20}$$

and streamline slope continuity. The pressure can be more conveniently expressed in terms of a pressure coefficient C_p, defined in terms of the pressure change from freestream divided by the upstream dynamic head. A linearized C_p model then can be used to separate out the axisymmetric component of each mode ($\bar{C}_{pk}$).

$$\bar{C}_{p_k}(r,x) = -2g_{x_k}(r,x) \tag{21}$$

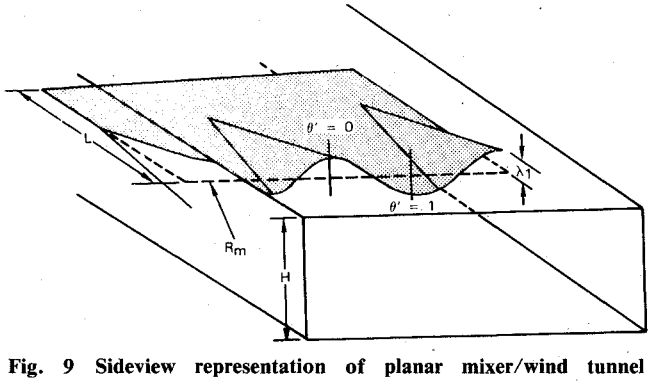

Fig. 9 Sideview representation of planar mixer/wind tunnel geometry.

At the lobe trailing edge, Eqs. (20) and (21) are equivalent to separate Kutta conditions for each mode separately. The streamline slope matching conditions along the general wake contour can also be simplified by assuming that the axial velocity flux contribution is small relative to unity and that the wake follows the constant radius approximation. Equations (18), (20), and (21) are then combined to determine the potential jump

$$[g_k]_x = 0 \tag{22}$$

Therefore, the jump in potential along the wake is determined solely by the jump at the trailing edge for the unpowered case. It is felt that an algorithm could be extended to permit the wake position to change with iteration algorithm and thereby converge to its actual location.

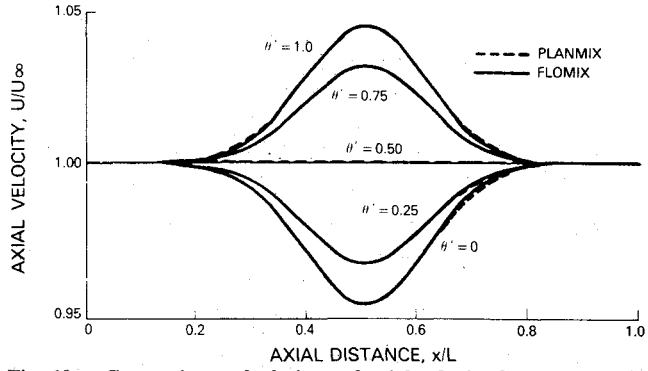

Fig. 10a Comparison calculations of axial velocity for a symmetric planar mixer in a planar duct.

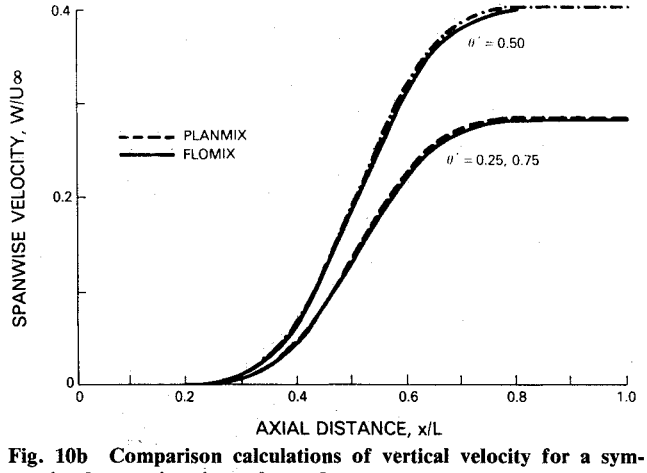

Fig. 10b Comparison calculations of vertical velocity for a symmetric planar mixer in a planar duct.

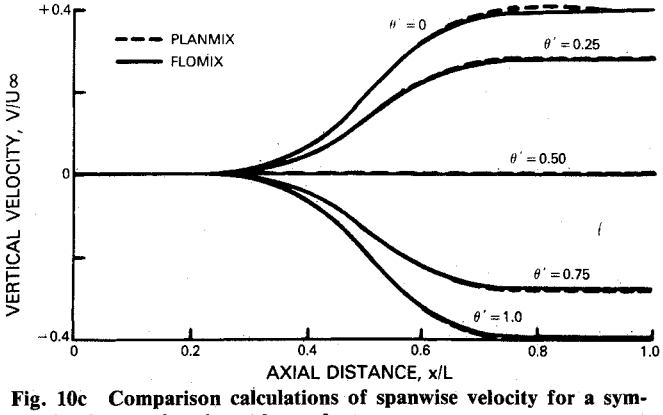

Fig. 10c Comparison calculations of spanwise velocity for a symmetric planar mixer in a planar duct.

Results and Discussion

The analysis, known as FLOMIX, described in the previous section has been applied to several configurations. When $\lambda_k = 0$ ($k = 1, 2, \ldots NH$), the zeroth mode solution will describe the flow over a completely axisymmetric configuration. An initial demonstration calculation for an axisymmetric unpowered afterbody/splitter configuration is presented to illustrate the Cartesian algorithm. The configuration analyzed with the corresponding predicted surface static pressures are shown on Fig. 8. The C_p difference between the upstream flows, arising from radial equilibrium effects, disappears when the plug inlet radius is large. The splitter surface C_p's at the trailing edge are forced to coincide by the Kutta condition.

A more interesting three dimensional calculation is considered below where comparison with a planar mixer lobe in a straight duct are presented to calibrate the model analysis. Planar conditions are simulated by considering an axisymmetric geometry at large radius. Comparison calculations have been made with a method that simulates an isolated planar mixer lobe with distributed doublets along a mean planar surface. This analysis, referred to a PLANMIX, was developed by Amiet.[8] Figure 9 shows a sideview of the configuration analyzed. The duct walls are defined sufficiently far from the lobes so that any interaction with them is minimal. Numerical calculations confirm that there is no potential interaction effect due to these walls. The lobe surface in both calculation methods is generated by a single cosine wave, therefore a single modal ($NH = 1$) solution models the flowfield. In this study no power addition effects are considered. Predictions are presented for the reconstructed (as a function of θ) components of the perturbation velocity on the lobe surface. The comparison calculations presented on Figures 10a-c, show excellent agreement between FLOMIX and PLANMIX for the three velocity components at several azimuthal or spanwise cuts running from other lobe crest ($\theta' = 0$) to inside the lobe trough ($\theta' = 1.0$). The normalized axial scale runs from the lobe leading edge to its trailing edge. The profiles reflect the effect of the linear theory approximations at the trailing edge, i.e., the Kutta condition is satisfied and the axial velocity perturbation goes to zero. Although both methods are based on linear theories, slight differences should be expected since the planar analysis is an inverse method which numerically evaluates singular integrals while the present method is a finite flux volume scheme.

Conclusions

The three-dimensional flow analysis for lobed forced mixers has been formulated. The analysis assumes that the flow processes are predominantly inviscid and that for slender mixer lobes ($\Delta R/L \ll 1$), the analysis can be uncoupled into a series of axisymmetric problems solved using a finite volume scheme on a Cartesian grid. The algorithm has been verified in separate calculations using a classical singularity superposition method.

The analysis also demonstrated that the Cartesian approach, with its simplicity and adaptability to problems involving complex geometries in two- or three-dimensions, can be efficiently used to analyze problems of engineering interest.

Acknowledgments

The authors wish to thank the NASA Lewis Research Center for sponsoring this work. The program, Contract number NAS3-23039, is under the direction of Mr. Allan Bishop. The authors also wish to thank Mr. D. Golden and Dr. W. C. Chin for their early contributions to the development of this analysis.

References

[1]Kuchar, A. P. and Chamberlin, R., "Scale Model Performance Test Investigation of Exhaust System Mixes for an Energy Efficient Engine (E^3) Propulsion System," AIAA Paper 80-0229, 1980.

[2]Kuchar, A. P. and Chamberlin, R., "Scale Model Performance Test Investigation of Mixed Flow Exhaust Systems for an Energy Efficient Engine (E^3) Propulsion System," AIAA Paper 81-0541, 1983.

[3]Kozlowski, H. and Kraft, G., "Experimental Evaluation of Exhaust Mixers for an Energy Efficient Engine," AIAA Paper 80-1088, 1980.

[4]Paterson, R. W. and Werle, M. J., "Turbofan Forced Mixer Flow Field," United Technologies Research Center, East Hartford, CT, UTRC R79-912924, 1979.

[5]Paterson, R. W., "Turbo Forced Mixer—Nozzle Internal Flow Field, I—A Benchmark Experimental Study," NASA CR3492, 1982.

[6]Golden, D. P., Barber, T. J., and Chin, W. C., "An Axisymmetric Nacelle and Turboprop Inlet Analysis Including Power Simulation," *Journal of Aircraft*, Vol. 20, June 1983, p. 536.

[7]Wedan, B., and South, J. C., "A Method for Solving the Transonic Full Potential Equation for General Configurations," AIAA Paper 83-1889, 1983.

[8]Amiet, R. K., "Users Manual for Task I—Laterally Planar Inviscid Mixer Analysis," Pratt & Whitney Aircraft, East Hartford, CT, Contract NAS3-23039, PWA-5904-18, 1983.